Navigation and Mission Design for Low-Thrust Insertion into Near Rectilinear Halo Orbits

Ethan W. Kayser[1], Michael R. Thompson[2], Matthew J. Bolliger[1], Nathan P. Ré[3]
Advanced Space, LLC, Westminster, Colorado, 80234, United States

Diane C. Davis[4]
ai solutions, Houston, Texas, 77058, United States

Melissa L. McGuire[5], Steven L. McCarty[6]
NASA Glenn Research Center, Cleveland, Ohio, 44135, United States

Near Rectilinear Halo Orbits, the target of NASA's Gateway, are slightly unstable and therefore require minimal insertion delta-V. This makes insertion using highly efficient low-thrust systems a viable and attractive option; however, it also may require the spacecraft to approach the insertion on a dynamically sensitive trajectory with multiple perilune passes. This study focuses on a low-thrust NRHO insertion from a spiral-out, Earth-to-Moon transfer that involves this type of dynamically sensitive approach. Correction maneuver and navigation strategies are found that are robust to initial state, navigation, and maneuver execution errors prior to and through insertion. Further, it is demonstrated that these maneuver and navigation strategies allow the spacecraft to transition to nominal NRHO stationkeeping after insertion, without the need for specially designed clean-up maneuvers or a significant amount of additional delta-V.

Introduction

Near Rectilinear Halo Orbits (NRHOs) are a subset of L1 and L2 halo orbits which are slightly unstable [1, 2]. This stability characteristic makes spacecraft with low-thrust systems a viable option for missions to NRHOs given the minimal delta-V required for insertion, which is typically the mission event requiring the most change in velocity in the least amount of time. This study covers pre-insertion correction maneuver targeting strategies, insertion maneuver sensitivity to pre-insertion state errors and maneuver execution errors, and the post-insertion transition to nominal NRHO stationkeeping. These strategies are analyzed for a specific low-thrust, spiral-out from Earth orbit, the Co-Manifested Vehicle (CMV) Design Reference Mission 3 (DRM-3). In addition to the maneuver design and targeting methods, navigation strategies are presented to bound the uncertainty for maneuver designs.

---

[1] Astrodynamics and Mission Design Engineer, AIAA member
[2] Navigation and Astrodynamics Engineer, AIAA member
[3] Optimization Lead, AIAA member
[4] Principal Systems Engineer, AIAA Associate Fellow
[5] Chief, Mission Architecture and Analysis Branch (LSM), PPE MD Team Lead
[6] PPE MD Lead Engineer, Mission Architecture and Analysis Branch (LSM)

I. Design Reference Mission 3 Ballistic and Insertion Phases

Design Reference Mission 3 (DRM-3) is the current design reference mission for the first two elements of NASA's Gateway: The Power and Propulsion Element (PPE) and the Habitation and Logistics Outpost (HALO) [3]. Together, these elements make up the Co-Manifested Vehicle (CMV). The DRM-3 utilizes low-thrust to transfer the CMV from a 200 km x 33,900 km altitude Earth-orbit to the Near Rectilinear Halo Orbit. The mission design consists of 4 phases: Spiral, Alignment, Ballistic, and Insertion. This study focuses on the navigation and trajectory correction maneuvers during the Ballistic and Insertion phases, as well as the transition to nominal stationkeeping operations in the NRHO.

The Ballistic Phase of the DRM-3 consists of a 39.3-day coast, during which the CMV nominally has no planned thrust events. This phase includes a dynamically sensitive, 3-revolution "wind-on", with 4 perilune passes. This mission phase is represented in white in Fig. 1. The Insertion Phase of the DRM-3 consists of two low-thrust insertion maneuvers, with burn durations of 3.0 and 1.4-days, and a 33.2-hour coast between them. This phase is represented in red in Fig. 1.

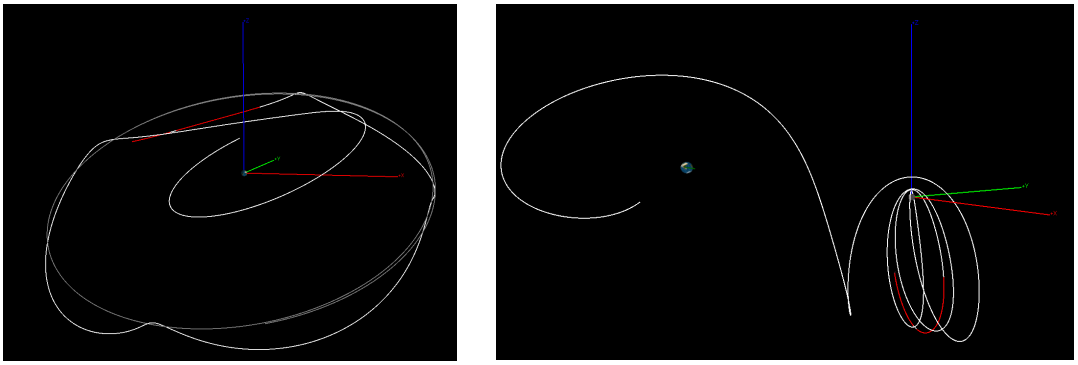

Fig. 1 Ballistic (white) and Insertion (red) Phases of the Design Reference Mission 3, in the Earth-centered J2000 inertial frame (left) and Moon-centered Earth-Moon rotating frame (right).

Due to the dynamically sensitive nature of the Ballistic Phase, trajectory correction maneuvers will be required to correct for state errors at the beginning of this mission phase. Fig. 2 illustrates a sample of 200 uncontrolled trajectories that begin with initial state errors offset from the reference trajectory by 10 km and 10 cm/s (3σ) in each cartesian direction. These states are then propagated to the start of the first insertion maneuver of the Insertion Phase. During this 39.3-day uncontrolled propagation, the state errors from the reference can grow to nearly 10,000 km and 100 m/s.

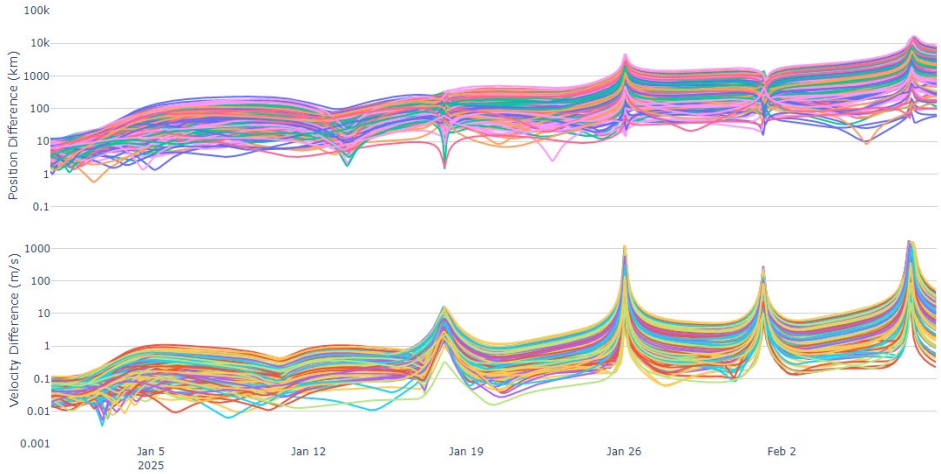

Fig. 2 Uncontrolled propagation of small initial state errors through the Ballistic Phase

II. Insertion Maneuvers

Before designing a trajectory correction maneuver strategy for the Ballistic Phase, it is important to bound the pre-insertion state errors by studying the sensitivity of the Insertion Phase itself. This analysis begins at the start of the first insertion maneuver, with initial state errors offset from the DRM-3. The insertion maneuvers, as defined in the DRM-3, are then executed with the maneuver execution errors outlined in Table 1. These maneuver execution errors are re-sampled and applied to the maneuver for 30-minute spans. Fig. 3 compares the pre-insertion state errors with the post-insertion state errors from the reference. Pre-insertion state errors are sampled from 10 km, 10 cm/s and 50 km, 50 cm/s (3σ) distributions, applied in each cartesian direction. These results illustrate that the post-insertion state errors are dominated by pre-insertion state errors, while maneuver execution errors seem to have little effect.

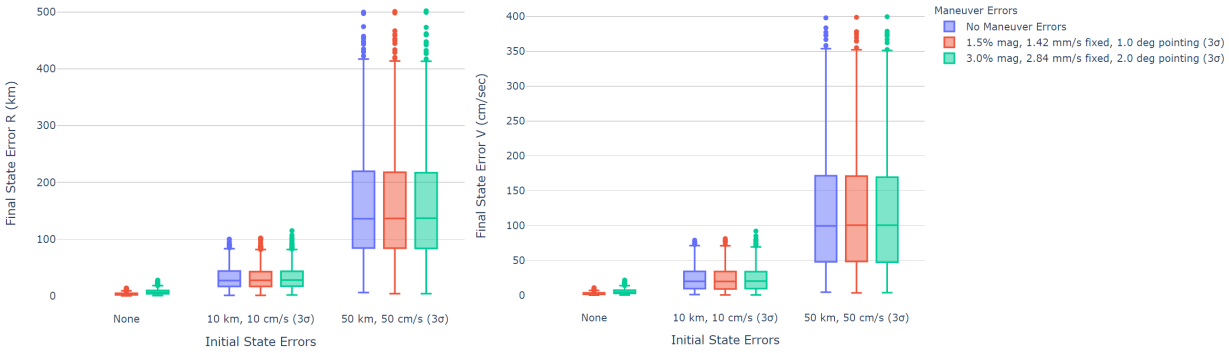

Fig. 3 Post-insertion position (right) and velocity (left) errors as a function of pre-insertion initial state errors and maneuver execution errors.

This same analysis is repeated but with a variety of maneuver error sample rates. Rather than re-sample the maneuver execution errors every 30-minutes, the errors are re-sampled every 60, 120 and 240-minutes. These results are shown in Fig. 4, and further illustrate that the Insertion Phase is most sensitive to pre-insertion state errors and robust to maneuver execution errors.

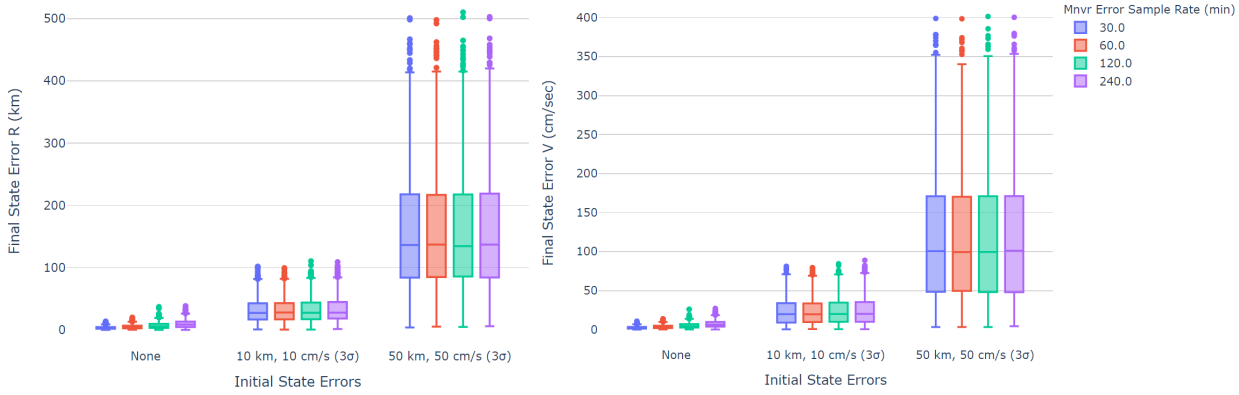

Fig. 4 Post-insertion position (right) and velocity (left) errors as a function of pre-insertion initial state errors and maneuver error sample rate.

To further understand how pre-insertion state errors relate to post-insertion state errors, scatter plots are produced which compare pre-insertion position (R) and velocity (V) errors with post-insertion position and velocity errors. In Fig. 5, it is shown that while both pre-insertion position and velocity errors contribute to post-insertion position and velocity errors, there is a stronger correlation between pre-insertion velocity errors and post-insertion position errors than between any other pair of parameters. This sensitivity suggests that the Ballistic Phase trajectory correction strategy should prioritize minimizing the velocity errors from the reference at the start of the first insertion maneuver.

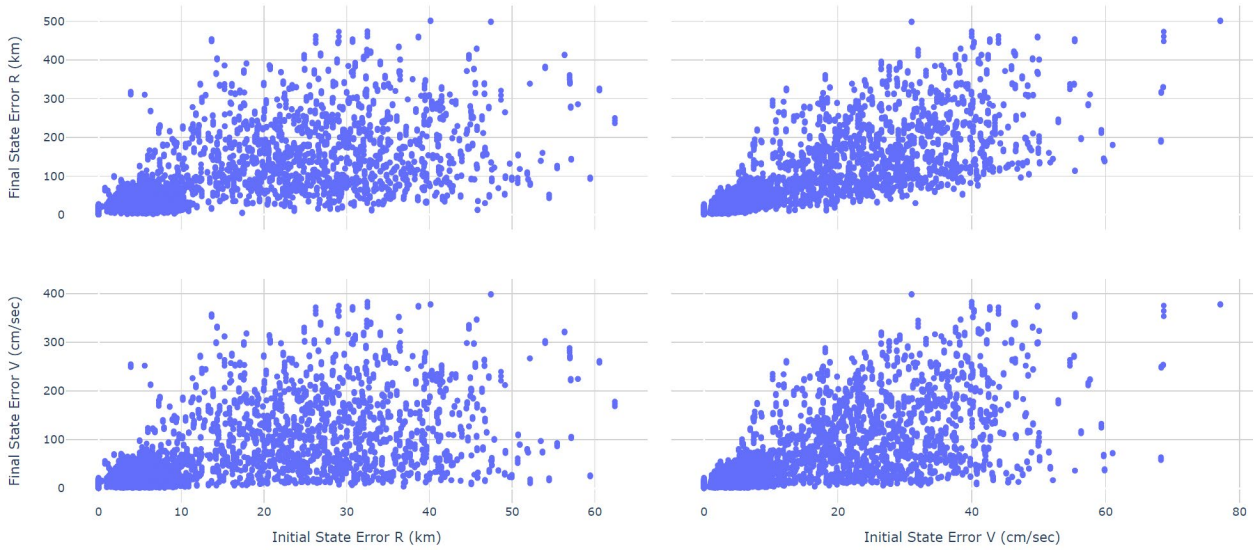

Fig. 5 Post-insertion final position and velocity errors vs. pre-insertion initial position and velocity errors

III. Targeting Insertion with Trajectory Correction Maneuvers

Due to the sensitivity of the ballistic trajectory and insertion maneuvers, trajectory correction maneuvers (TCMs) must be planned and executed to ensure the spacecraft can successfully achieve the NRHO. Several Monte Carlo simulations are conducted to understand the ideal number and placement of these TCMs, as well as assess their sensitivity to initial state, navigation, and maneuver execution errors. Each simulation begins with a set of spacecrafts offset from the DRM-3 at the start of the Ballistic Phase. TCMs are then planned with incorrect state knowledge by propagating navigation errors forward from a 24-hour data-cutoff. These state knowledge errors are sampled from the covariances provided by the navigation analyses described in a subsequent section. Each TCM targets the position of the reference at the epoch of the next TCM (except for the final TCM, which targets the position of the reference at the start of the first insertion maneuver). These TCMs are then executed as finite maneuvers with maneuver execution errors. Finally, the two low-thrust insertion maneuvers, as defined in the DRM-3, are executed with maneuver execution errors. Unless otherwise specified, the simulations use continuous navigation tracking and the baseline errors in Table 1.

Table 1 Baseline errors for the Ballistic Phase trajectory correction maneuver analysis

Baseline Initial State Errors	
Parameter	**3σ Error**
Position (in each cartesian direction)	10 km
Velocity (in each cartesian direction)	10 cm/s

Baseline Maneuver Execution Errors	
Parameter	**3σ Error**
Thrust Magnitude Proportional	1.5%
Thrust Magnitude Fixed	1.42 mm/s
Pointing	1°

A variety of TCM cadences are tested in these simulations. Prior to the wind-on subphase of the ballistic trajectory, 0-3 maneuvers are placed (7, 4 or 3 days apart) to clean up initial state errors. Then, during the wind-on subphase, maneuvers are placed at every or every-other apolune (approximately 6.5 or 13.5 days apart), following the effectiveness of the nominal NRHO stationkeeping strategy [4]. In a few of the candidate TCM cadences, two maneuvers are placed around either the first or last apolune of the wind-on sub-phase ("Split First" or "Split Last", respectively). Each TCM cadence is illustrated and given a short-hand name in Fig. 6.

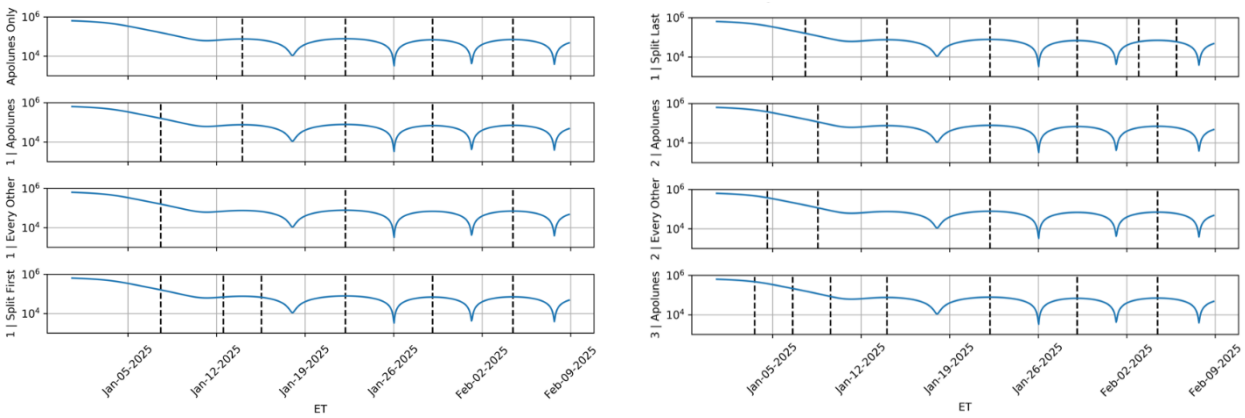

Fig. 6 CMV distance from the Moon during the Ballistic Phase. Candidate trajectory correction maneuver cadences are shown as vertical dashed lines

TCM cadences are evaluated by their achieved pre-insertion state error (i.e., the difference between the spacecraft's state and reference trajectory's state at the start of the first low-thrust insertion maneuver), as well as their robustness to navigation cadences, maneuver execution errors and initial state errors. For brevity, only pre-insertion velocity errors are shown, as the results from the previous section suggest that post-insertion state errors are most affected by pre-insertion velocity rather than position errors. In general, the trends of the pre-insertion position errors follow the same trends as the pre-insertion velocity errors.

Fig. 7 compares these pre-insertion velocity errors for the different combinations of maneuver and navigation cadences. More details on the navigation cadences can be found in section V. This figure shows that all the candidate TCM cadences, except the "Apolunes Only" cadence, achieve pre-insertion velocity errors that are consistently under 10 cm/s, even with the sparsest navigation cadence of just three 4-hour tracks per week. For most maneuver cadences, continuous tracking offers insignificant benefits compared to the hybrid tracking cadence, suggesting that one track per day prior to the wind-on is sufficient.

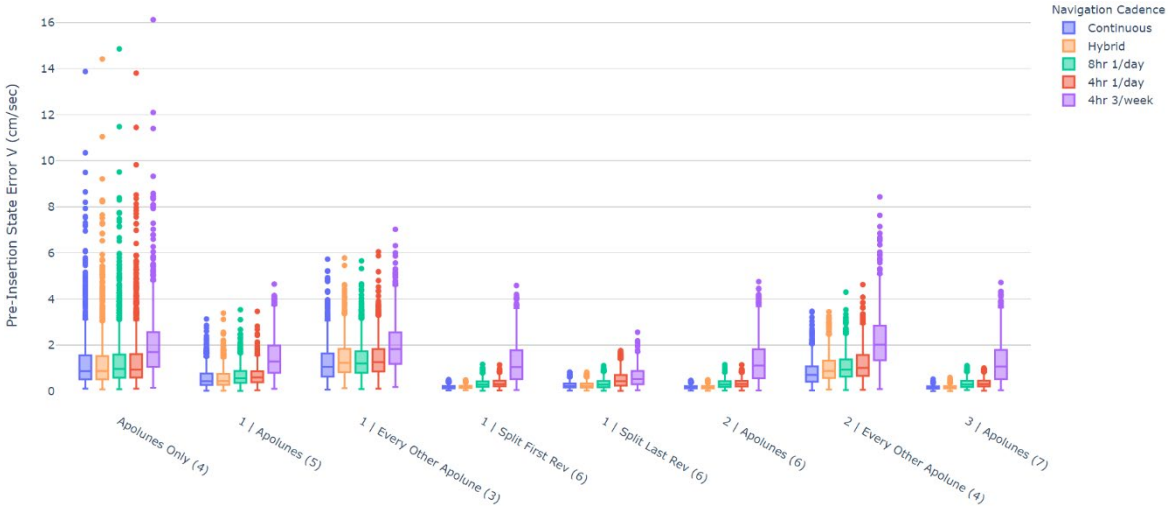

Fig. 7 Pre-insertion velocity error sensitivity to maneuver and navigation cadences. Integers in parentheses are the total number of TCMs for that maneuver cadence.

Next, the impact of larger maneuver execution errors on the pre-insertion velocity error is examined. Fig. 8 shows that although doubling the maneuver execution errors does increase pre-insertion state errors, as expected, the effect is minimal. This follows the trend in Fig. 3, and demonstrates that both the Ballistic and Insertion Phase are robust to maneuver execution errors.

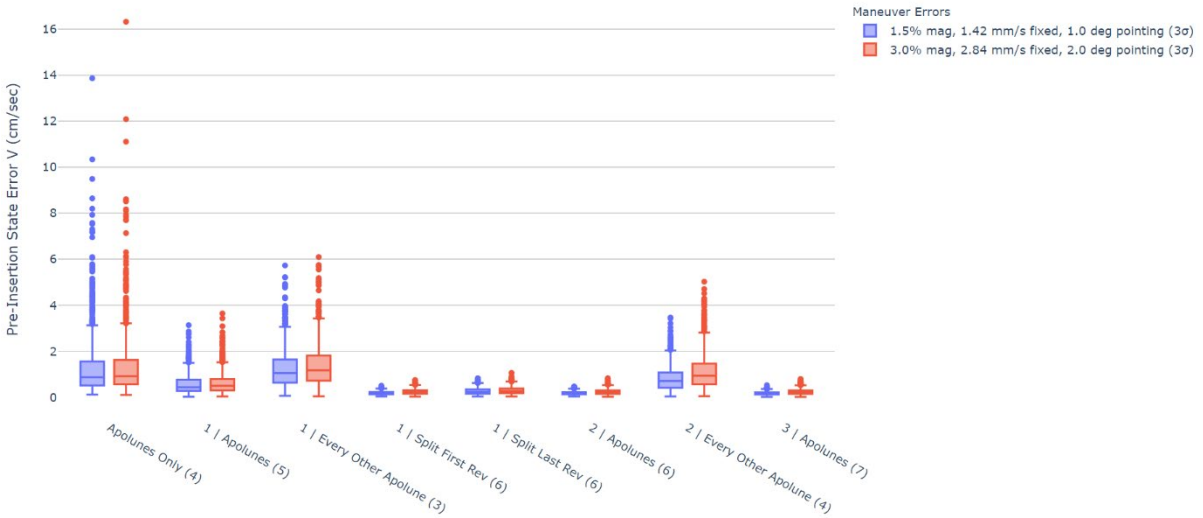

Fig. 8 Pre-insertion velocity error sensitivity to maneuver cadence and maneuver execution errors

While pre-insertion state errors are not sensitive to navigation or maneuver execution errors, the magnitude of the initial state errors applied at the beginning of the Ballistic Phase can significantly impact a maneuver cadences ability to achieve small pre-insertion state errors. In Fig. 9, it is shown that only three of the tested maneuver cadences are robust to 50 km, 50 cm/s (3σ) initial state errors: "1 | Split First Rev", "2 | Apolunes" and "3 | Apolunes". These cadences have a maneuver every apolune, and either more than one maneuver prior to the "wind-on", or, in the case of the "1 | Split First Rev" cadence, one maneuver prior to the "wind-on" and two around the first apolune. In general, to be robust to larger initial state errors, the state errors must be minimized prior to the "wind-on" with 2-3 maneuvers, then controlled with at least one additional TCM at each apolune. If maneuver execution errors are smaller, on the order of 20 km, 20 cm/s (3σ), pre-insertion velocity errors under ~10 cm/s can be achieved with just 3 or 4 TCMs, as is the case for the "1 | Every Other Apolune" and "2 | Every Other Apolune" cadences.

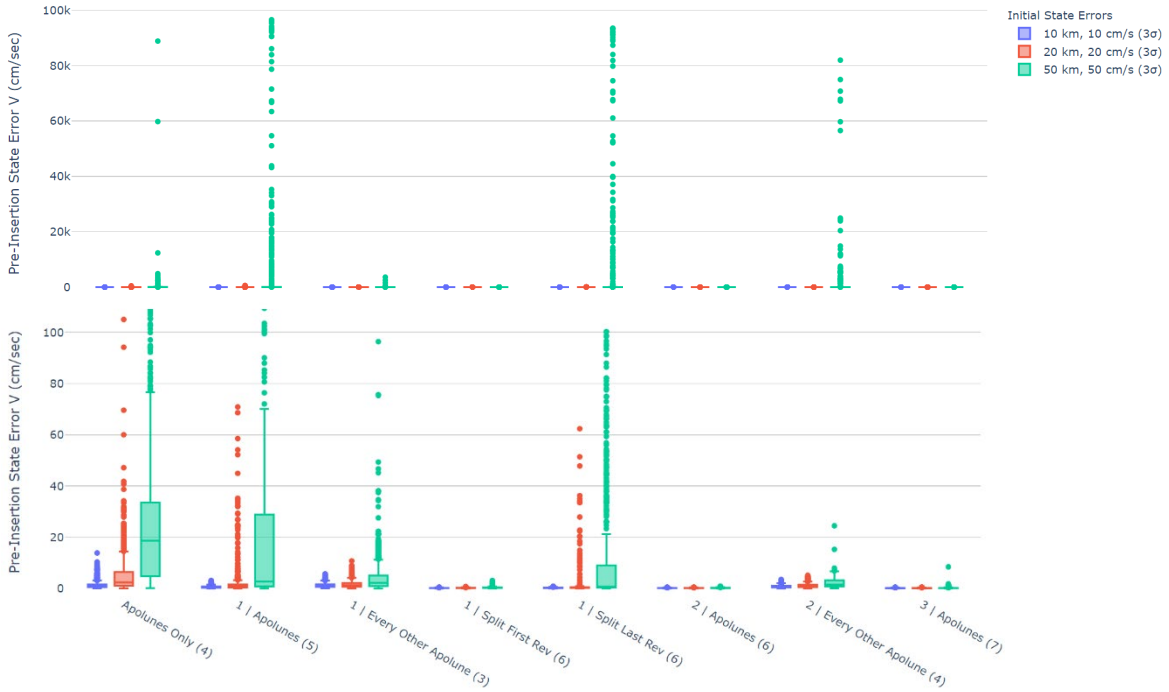

Fig. 9 Pre-insertion velocity error sensitivity to maneuver cadence and Ballistic Phase initial state errors. The top set of box plots shows all data points, while the bottom set of box plots zooms in on the range from 0 to 100 cm/s.

In addition to assessing the TCM cadences by analyzing the achieved pre-insertion state errors, the total ΔV for each strategy is considered. In Fig. 10 and Fig. 11, it is demonstrated that the total TCM ΔV is nearly independent of the navigation cadence and is mostly a function of the Ballistic Phase initial state errors and maneuver cadence.

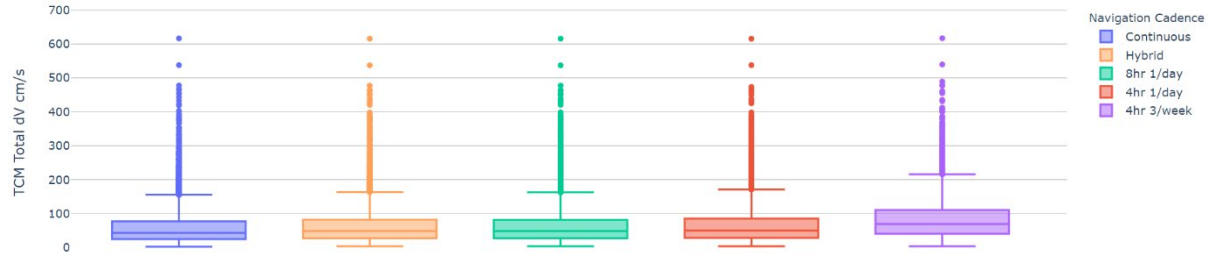

Fig. 10 TCM ΔV sensitivity to navigation cadence

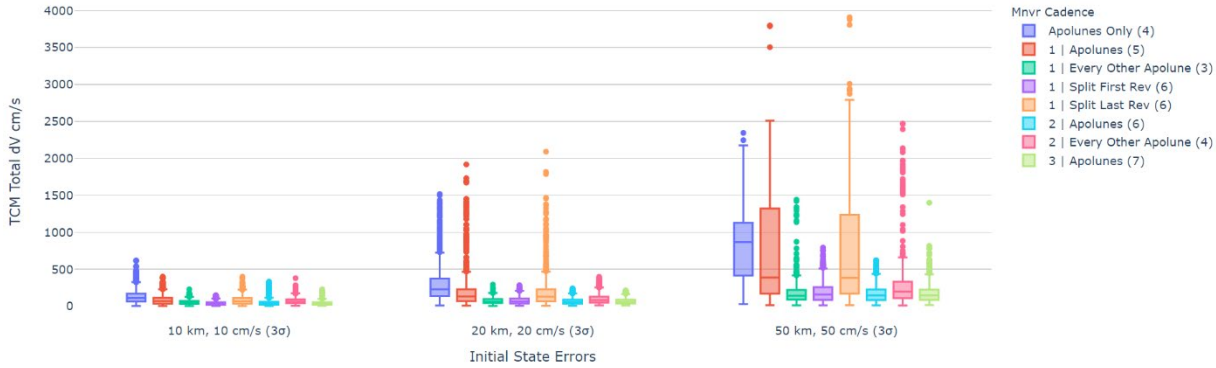

Fig. 11 TCM ΔV sensitivity to maneuver cadence and Ballistic Phase initial state errors

Based on the analyses described above, two TCM cadences are recommended depending on the magnitude of initial state errors. If the initial state errors are 50 km, 50 cm/s (3σ) or greater, two TCMs should be placed prior to the wind-on with the first placed four days after the start of the Ballistic Phase, and the second four days later. Then, a TCM should be placed at the apolune of each wind-on, for a total of six TCMs. This strategy is robust to the assumed initial state errors, and achieves minimal post-insertion state errors for less than ~500 cm/s. If the initial state errors are smaller, 20 km and 20 cm/s (3σ), minimal post-insertion state errors can be achieved with just four TCMs. Two placed four days apart prior to the wind-on, then one maneuver at every other apolune. This strategy utilizes less than 320 cm/s. The pre-insertion, post-insertion and next apolune state errors for each recommended TCM strategy, as well as the total ΔV cost, are presented in Table 2.

Table 2 State errors and TCM costs for recommended TCM cadences, using the Hybrid navigation cadence

Ballistic Phase Initial State Errors	Recommended TCM Cadence	Pre-Insertion State Error μ / P99		Post-Insertion State Error μ / P99		Next Apolune State Error μ / P99		TCM Cost (cm/s) μ / P99
		Position (km)	Velocity (cm/s)	Position (km)	Velocity (cm/s)	Position (km)	Velocity (cm/s)	
50 km, 50 cm/s (3σ)	2 | Apolunes	0.210 0.616	0.239 0.659	3.82 10.5	2.72 7.91	5.30 13.1	2.10 6.11	170 504
20 km, 20 cm/s (3σ)	2 | Every Other	1.66 8.64	1.26 3.96	6.44 24.1	4.75 18.0	6.72 21.0	3.05 9.98	105 318

Both recommended TCM cadences achieve next apolune state errors (i.e., the state difference between the truth trajectory and reference trajectory at the first apolune after insertion) on the order of 10 km, 10 cm/s (3σ). In the next

section, it is demonstrated that this distribution of state errors allows the CMV to transition immediately to nominal stationkeeping operations, requiring neither specially designed clean-up maneuvers nor a significant amount of additional ΔV.

IV. Transition to Nominal NRHO Stationkeeping

To determine whether additional correction maneuvers are needed after the Insertion Phase, Monte Carlo simulations are performed with a variety of truth and navigation initial state perturbations. The truth initial state perturbations are offsets of the spacecraft from the reference, while the navigation initial state perturbations are the state knowledge errors offset from the truth state of the spacecraft (and used to plan maneuvers). These initial state errors are applied at the first apolune following insertion. Each trial in the Monte Carlo is a high-fidelity simulation that includes simulated ground-based navigation with the DSN and Orbit Maintenance Maneuvers (OMMs) which are planned with incorrect state knowledge and executed with maneuver errors. OMMs are executed once per revolution of the NRHO. Details on this simulation set-up can be found in "Near Rectilinear Halo Orbit Determination with Simulated DSN Observations" [5]. Additional details on the Orbit Maintenance Maneuver method used, the "Short-horizon" strategy, can be found in "Phase Control and Eclipse Avoidance in Near Rectilinear Halo Orbits" [6].

In Fig. 12, OMM magnitudes for each revolution of the NRHO are presented for each trial of the Monte Carlo simulation. Even with large initial state errors (150 km, 75 cm/s 3σ in each cartesian direction), Fig. 12 shows that the ΔV magnitude of the OMMs reaches steady state behavior after just two revolutions. This suggests that specially designed clean-up maneuvers are not required, and that the CMV can transition to nominal stationkeeping operations immediately after insertion, albeit with larger OMMs during the first couple revolutions.

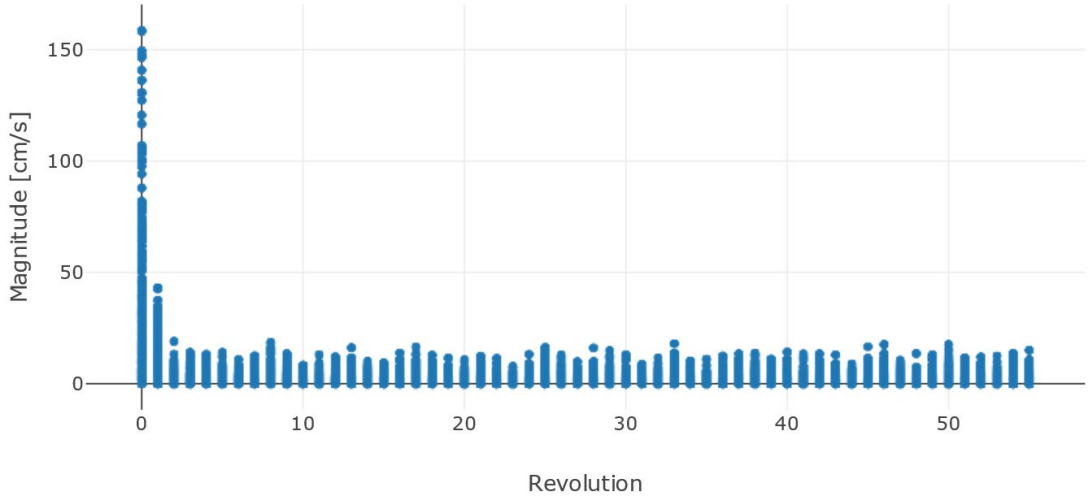

Fig. 12 Orbit Maintenance Maneuver ΔV magnitudes by revolution number in the NRHO. Revolution 0 corresponds to the first revolution after the Insertion Phase.

The ΔV magnitudes of first two OMMs, as expected, increase as the truth initial state errors increase. The cost of these first maintenance maneuvers seems to be less sensitive to navigation errors though, as illustrated in the box plots in Fig. 13 and mean-plus-3σ values in Table 3.

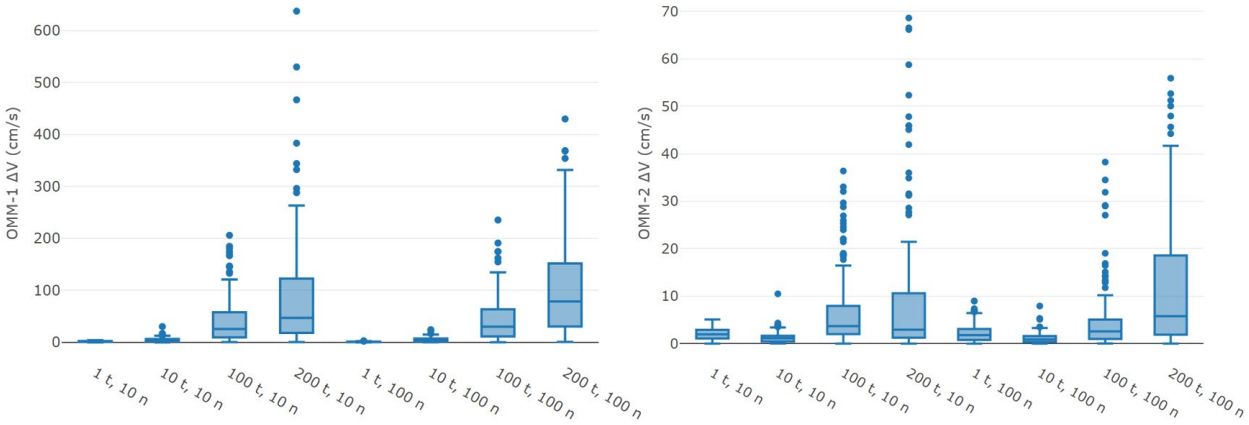

Fig. 13 ΔV distributions for the first two Orbit Maintenance Maneuvers after insertion (OMM-1 and OMM-2). Initial state truth (t) and navigation (n) errors in km, cm/s (3σ). See Table 3 for more details on the naming convention of each case.

Table 3 Mean and mean + 3σ ΔVs for the first two Orbit Maintenance Maneuvers (OMMs) after insertion

Figure Label	Initial State Errors (3σ)		OMM-1 (cm/s) μ / μ + 3σ	OMM-2 (cm/s) μ / μ + 3σ	Total (cm/s) μ / μ + 3σ
	Truth	Navigation			
1 t, 10 n	1 km, 1 cm/s	10 km, 10 cm/s	1.80 / 4.94	2.03 / 5.65	3.83 / 8.93
10 t, 10 n	10 km, 10 cm/s		4.92 / 16.8	1.32 / 5.04	6.24 / 20.0
100 t, 10 n	100 km, 100 cm/s		42.2 / 178	6.75 / 30.4	48.9 / 203
200 t, 10 n	200 km, 200 cm/s		88.0 / 408	9.57 / 53.8	97.6 / 450
1 t, 100 n	1 km, 1 cm/s	100 km, 100 cm/s	1.04 / 2.81	2.15 / 7.19	3.20 / 8.33
10 t, 100 n	10 km, 10 cm/s		5.44 / 18.6	1.16 / 4.52	6.61 / 20.5
100 t, 100 n	100 km, 100 cm/s		44.9 / 179	4.93 / 25.6	49.8 / 198
200 t, 100 n	200 km, 200 cm/s		103 / 372	12.7 / 56.1	116 / 419

The recommended navigation and TCM cadences, summarized in Table 2, achieve next-apolune state errors on the order of 10 km and 10 cm/s (3σ). Given the results in Table 3 the corresponding predicted cost for correcting the errors from the Ballistic and Insertion Phase is predicted to be approximately 20 cm/s (3σ).

V. Navigation

To provide state knowledge errors for the Ballistic Phase trajectory correction maneuver analysis, high-fidelity navigation analyses are performed with a selection of navigation cadences. For all analyses examined in this study, the navigation uncertainties are derived from realistic orbit determination simulations using simulated DSN tracking data. The orbit determination filters are written in JPL's Monte, and mimic the operational filters utilized for cislunar orbit determination at Advanced Space. The estimated filter parameters are given in Table 4.

Table 4 Data noise and per-pass biases.

Measurement	Cadence			Noise (1-sigma)	Per-Pass Bias (1-sigma)
Two-Way Range	1 per 60s			1 m	7.5 m
Two-Way Doppler	1 per 60s	0.1 mm/s	None		

Table 5 Estimated filter parameters.

Estimated Parameter	A-Priori Covariance (1-Sigma)	Update Cadence	Comments
State	10^2 km / 10^0 km/s	N/A	In each EME2000 direction.
SRP Scale Factor	0.1	N/A	Scale factor to model both area and reflectivity mismodeling.
TCM	0.5 % magnitude 0.33 deg pointing	N/A	Applied for each TCM.
Range Bias	7.5 m	Per-Pass	
Stochastic Accelerations	10^{-11} km/s^2	8 hr	

For these studies, the navigation simulation is beyond a simple covariance analysis. Instead, measurement observables are simulated with realistic noise values and stochastic biases (see Table 5), processed in an operational-like filter to generate trajectory estimates and covariance mappings, and passed into the maneuver design process. This end-to-end process provides a better model of reality than basic covariance studies.

For each TCM schedule studied (see Fig. 6), multiple navigation simulations are performed using five different potential navigation cadences. The five navigation cadences considered in this analysis are: continuous tracking, "hybrid", one 8-hour track per day, one 4-hour track per day, and three 4-hour tracks per week. The "hybrid" tracking cadence involves one 8-hour track per day prior to the final wind-on phase, and continuous afterwards. The outputs of these studies are a total of 40 different setups (8 TCM schedules and 5 tracking cadences) for which the instantaneous covariance can be computed.

One high-level takeaway from running this full set of cases is that the navigation uncertainty is *much* more dependent on the tracking cadence than the TCM schedule. That is, for a given tracking cadence, the instantaneous uncertainty throughout the ballistic arc is nearly constant across different TCM schedules. In these cases (consistent tracking cadence, differing TCM schedule), the only difference between individual cases is the positioning and magnitude of maneuver execution errors, which are inserted at each TCM. For large execution errors or maneuvers placed in dynamically sensitive areas, this can lead to large differences in the navigation uncertainty, but for this analysis, neither of these conditions are met. The studied TCM strategies all focus on placing maneuvers near apolune and have quite small maneuver execution errors based on the current set of assumptions being utilized by the Gateway navigation team. As a brief example, a TCM of 20 cm/s placed near apolune results in a maneuver execution error of 0.473 mm/s fixed and 1 mm/s proportional 3-sigma. Near apolune, where the sensitivity of the trajectory is somewhat low, this amount of injected uncertainty does not have a significant effect on the covariance growth. For cases with continuous or daily tracking, the covariance is quickly decreased back to its "steady-state" once the maneuver is estimated in the filter. For cases with more sparse tracking, there is some covariance growth until the next track, but the size of the maneuver execution error is not enough to significantly drive this increase.

A result of this finding is that as a first-order analysis, the navigation uncertainties can be examined mostly independent of the TCM schedule. Note that this takeaway is valid for the currently studied set of TCMs, which tend to be small and placed near apolune. It may not hold if the magnitude of the TCMs or maneuver execution errors are drastically increased or if TCMs are placed closer to perilune passages.

The instantaneous covariance during the ballistic arc for one given TCM schedule and varying tracking cadences is shown in Fig. 14 and Fig. 15.

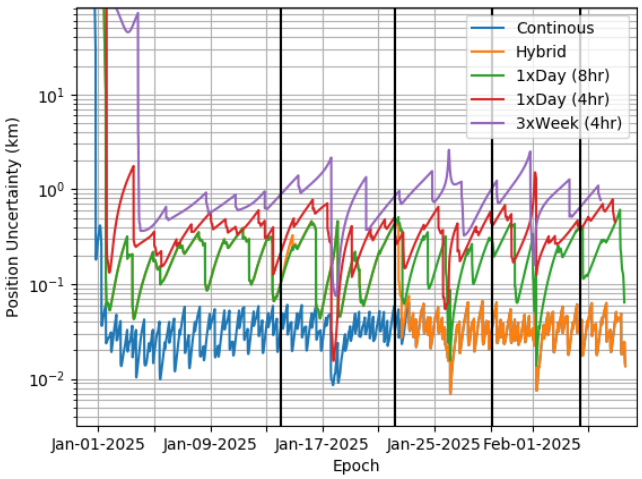

Fig. 14 Instantaneous position uncertainties (3σ) for multiple tracking cadences during the Ballistic Phase. TCM locations are marked by vertical black lines.

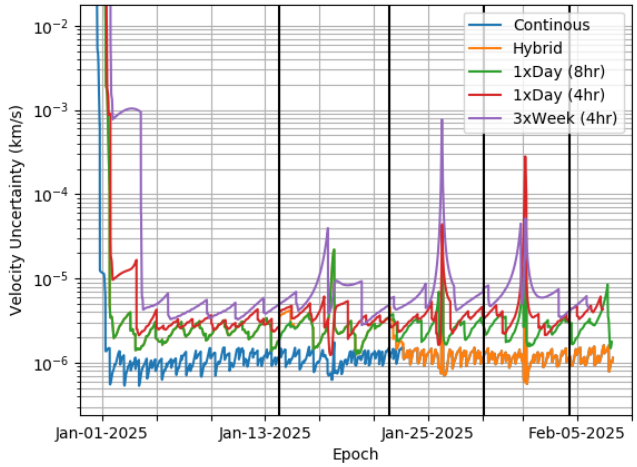

Fig. 15 Instantaneous velocity uncertainties (3σ) for multiple tracking cadences during the Ballistic Phase. TCM locations are marked by vertical black lines.

As seen in these figures, there is no appreciable increase in the covariance due to the TCMs themselves, which are marked as vertical black lines. The instantaneous navigation uncertainty is driven primarily by the dynamics and tracking schedule. While there are expected spikes in the velocity covariance near perilune passages, the "steady-state" values remain at a roughly consistent order of magnitude throughout the ballistic arc. The time-based average of the navigation uncertainty through the entire ballistic phase are computed for each combination of TCM cadence and tracking cadence. These results are shown in Table 6.

Table 6 Time-based average 3-sigma navigation uncertainties through the Ballistic Phase, computed post filter convergence (meters, millimeters/second)

TCM Cadence	Tracking Cadence				
	Continuous	Hybrid	1 8-hr track/day	1 4-hr track/day	3 4-hr tracks/week
0 | Apolunes	33.0 / 1.18	127 / 2.05	208 / 2.78	374 / 4.50	831 / 8.65
1 | Apolunes	33.0 / 1.18	128 / 2.08	208 / 2.78	375 / 4.59	838 / 8.70
1 | Every Other	33.0 / 1.18	126 / 2.04	208 / 2.78	373 / 4.46	835 / 8.67
1 | Split First	33.0 / 1.18	127 / 2.07	208 / 2.81	374 / 4.47	850 / 8.83
1 | Split Last	33.0 / 1.18	128 / 2.08	208 / 2.78	369 / 4.46	838 / 8.70
2 | Apolunes	33.1 / 1.19	128 / 2.08	208 / 2.78	376 / 4.52	837 / 8.68
2 | Every Other	33.1 / 1.19	127 / 2.04	208 / 2.78	374 / 4.49	835 / 8.65
3 | Apolunes	33.0 / 1.18	128 / 2.08	208 / 2.81	375 / 4.53	858 / 8.87

The time-based average results shown in Table 6 demonstrate that for all of the examined TCM cadences, the CMV can be tracked to a 3-sigma navigation uncertainty of (on average) within 1 km and 1 cm/s. Even with a relatively sparse tracking case (3 tracks of 4-hr per week), navigation uncertainties are kept quite low. Given this, with the current assumptions of TCM schedules, maneuver execution errors, and radiometric measurement quality, the tracking schedule will most likely be driven by mission operations requirements and not mission design / navigation requirements during this phase of the transfer.

In addition to estimating the instantaneous covariance in the navigation filter, mapping the uncertainty covariance to a future epoch, such as the epoch of the start of the insertion burn, can provide insight into how the knowledge of the spacecraft state at insertion changes throughout the pre-insertion revolutions. The uncertainty on the state at the start of the insertion burn is shown in Fig. 16 and Fig. 17 for the same tracking cadences examined previously.

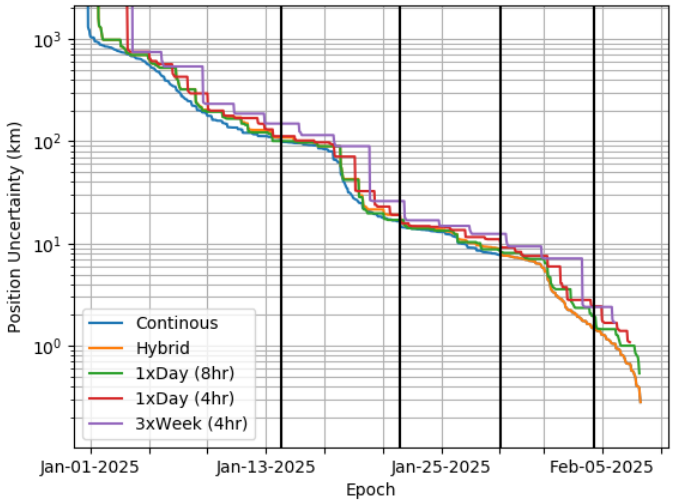

Fig. 16 Position covariance (3σ) mapped to the insertion burn epoch.

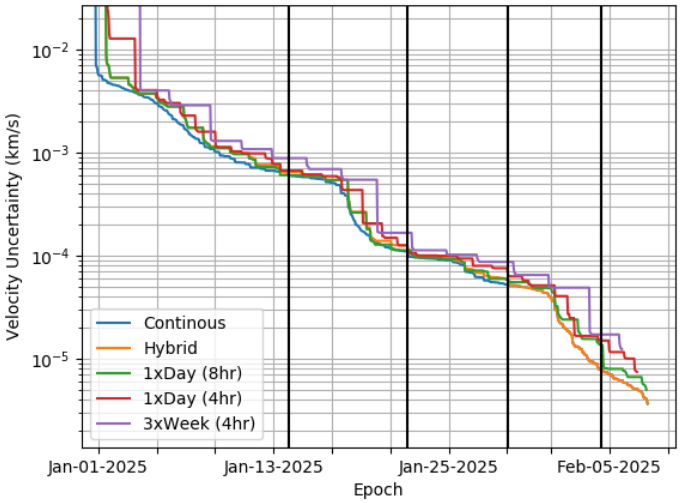

Fig. 17 Velocity covariance (3σ) mapped to the insertion burn epoch.

These mappings to the epoch of the insertion burn show the uncertainty on the state throughout the ballistic arc. The vertical black lines are once again TCMs for this specific setup. If the TCMs were large or in more dynamically sensitive locations, there would be an associated drop in the insertion state uncertainty once the spacecraft passed them. However, as previously discussed, this is not the case for the currently examined TCM strategy. Instead, the downstream uncertainty is dominated by the natural dynamics of the system, and the largest drops in the insertion burn uncertainty quickly occur after each perilune passage during the wind-on phase.

VI. Conclusion

The analyses in this paper demonstrate that although low-thrust insertion into Near Rectilinear Halo Orbits is dynamically sensitive, appropriately designed trajectory correction maneuver and navigation strategies can provide an accurate insertion that doesn't require specially designed, post-insertion clean-up maneuvers or a significant amount of additional ΔV. Both the Ballistic and Insertion Phases of the DRM-3 are found to be robust to both maneuver execution errors and the amount of ground-based tracking, but sensitive to both initial state errors and the number and placement of correction maneuvers.

Acknowledgments

The authors wish to acknowledge support from the NASA SBIR (Small Business Innovative Research) program and Caltech for the use of Monte software.

References

[1] Howell, K. C., Breakwell, J. V. "Almost Rectilinear Halo Orbits," *Celest. Mech*, 1984.

[2] Zimovan, E. M., Howell, K. C., Davis, D. C., "Near Rectilinear Halo Orbits and Their Application in Cis-Lunar Space," IAA/AAS SciTech Forum, 2017. IAA-AAS-DyCoSS3-125

[3] McGuire, M. L., McCarty S. L., et al., "Overview of the Lunar Transfer Trajectory of the Co-Manifested First Elements of NASA's Gateway" AAS/AIAA Astrodynamics Specialist Conference, Big Sky, Virtual, Aug 2021. AAS 21-697.

[4] Davis, D. C., S. A. Bhatt, K. C. Howell, J. Jang, R. L. Whitley, F. D. Clark, D. Guzzetti, E. M. Zimovan, and G. H. Bartond, "Orbit Maintenance and Navigation of Human Spacecraft at Cislunar Near Rectilinear Halo Orbits," 27th AAS/AIAA Space Flight Mechanics Meeting, San Antonio, Texas, February 2017.

[5] Parrish, N. L., Bolliger, M. J., Kayser, E., Thompson, M. R., Parker, J. S., Cheetham, B. W., Davis, D. C., Sweeney, D. J. "Near Rectilinear Halo Orbit Determination with Simulated DSN Observations," AIAA Scitech 2020 Forum, Orlando, FL, Jan 2020. AIAA 2020-1700.

[6] Davis, D. C., Khoury, F. S., Howell, K. C., Sweeney, D. J., "Phase Control and Eclipse Avoidance in Near Rectilinear Halo Orbits," AAS/AIAA Astrodynamics Specialist Conference, Lake Tahoe, CA, Aug 2020. AAS 20-047.